Scalp Acupuncture Protects Against Neuronal Ferroptosis by Activating the P62-Keap1-Nrf2 Pathway in ICH Rat Models

Ming yue Li (1529475735@qq.com)
The First Affiliated Hospital of heilongjiang university of traditional chinese medicine
https://orcid.org/0000-0003-0793-911X

Xiaohong Dai
The First Affiliated Hospital of heilongjiang university of traditional chinese medicine

Xueping Yu
The First Affiliated Hospital of Heilongjiang traditional chinese medicine

Wei Zou
Department of Neurology,First Affiliated Hospital,Heilongjiang University of Chinese Medicine,Harbin,Heilongjiang Province,China

Wei Teng
The first affiliated hospital of heilongjiang university of traditional chinese medicine

Peng Liu
The first affiliated hospital of heilongjiang university of traditional chinese medicine

Xinyang Yu
Clinical Key Laboratory of Integrated Traditional Chinese and Western Medicine ,heilongjiang University of Chinese medicine

Qi An
Heilongjiang University of Traditional Chinese Medicine: Heilongjiang University of Chinese Medicine

Xin Wen
Heilongjiang University of Chinese Medicine

Research Article

Keywords: intracerebral hemorrhage, scalp acupuncture, ferroptosis, P62,Nrf2,GPX4, FTH1

Posted Date: April 26th, 2021

DOI: https://doi.org/10.21203/rs.3.rs-427035/v1

Version of Record: A version of this preprint was published at Journal of Molecular Neuroscience on August 17th, 2021. See the published version at https://doi.org/10.1007/s12031-021-01890-y.

Abstract

Intracerebral hemorrhage (ICH) is a devastating disease and different patients have varying degrees of neurological impairment despite after treatment. However, the therapeutic strategies targeting currently known cell death pathways of the secondary injury fail to effectively improve neurological deficits after ICH. As a new form of cell death, ferroptosis is closely related to neurological deficits after ICH. Moreover, increasing evidence has shown that scalp acupuncture (SA) has a neuroprotective effect on ICH rats by mediating different molecular pathways. Our study sought to investigate the effect of SA treatment on neurological function and elucidate whether SA could alleviate secondary injury after ICH by regulating ferroptosis, alongside analyzing its underlying mechanisms. First, our results demonstrated that SA treatment (Baihui [DU20] acupoint-penetrating-Qubin [GB7] acupoint, on the lesion side) could attenuate neurological functional impairment in ICH rats, according to the Ludmila Belayev test, and improve pathological injury according to hematoxylin-eosin staining. Second, perihematomal brain tissues from different groups were collected to detect the biological characteristics of neuronal ferroptosis including iron overload, lipid peroxidation accumulation, mitochondrial morphology changes and the decreased NeuN expression levels. Results revealed that SA treatment could attenuate neuronal ferroptosis in ICH rats to a remarkable degree. Furthermore, consistent with deferoxamine (DFX) being one of the main inhibitors of ferroptosis, there were no significant differences between the effects of SA treatment and DFX administration. The molecular mechanism studies found that SA treatment triggered the antioxidant effect alongside activating the p62/Keap1/Nrf2 pathway and up-regulating levels of ferritin heavy chain 1 (FTH1) and glutathione peroxidase 4 (GPX4), which contributed to reduced iron overload and oxidative stress in ICH rats. These results suggest that the p62/Keap1/Nrf2 signaling pathway is responsible for alleviating ferroptosis lipid peroxidation injury after ICH, thereby providing new theoretical basis with regards to SA treatment of ICH.

Introduction

Intracerebral hemorrhage (ICH) is one of the leading diseases that is a serious threat to human life, characterized by high rates of morbidity, disability and fatality, and is responsible for nearly 15% of all strokes in the United States each year(Haller et al., 2019). According to global epidemiological data, the total incidence of ICH is of 24.6 in one hundred thousand people, with an even higher incidence in Asian populations(Weimar et al., 2017). Although some progress has been made in the treatment of acute cerebral hemorrhage, disability and mortality rates remain relatively high. Existing treatment methods are insufficient to correct the neuron injury or death after ICH(Rocha et al., 2020).It is urgent to provide a new treatment and understand its molecular mechanism.

Recently, studies have shown that ferroptosis is important to neuronal survival(Buccarelli et al.,2018). It differs from other forms of regulated cell death by virtue of its unique process of Fe^{2+}-dependent lipid peroxidation. An imbalance in iron homeostasis and lipid peroxidation-associated damage are considered key events linked to ferroptosis(Müller et al.,2017). Although ferroptosis was first described in cancer cells, it plays a similar role in neurons(Zille et al.,2019). Increasing evidence link the mechanisms

of ferroptosis to nervous system diseases, such as Alzheimer's disease (AD), Parkinson's disease, Huntington's disease, and Amyotrophic lateral sclerosis (ALS) (Devos et al.,2019;Masaldan et al.,2019;DeGregorio-Rocasolano et al.,2019). In addition, experimental evidence has suggested that ferroptosis also occurs in stroke(Qinqin et al.,2020), including cerebral ischemia and brain hemorrhage(Li et al.,2017;Zhang et al.,2018). Following intracerebral hematoma formation, excessive amounts of iron were produced by the breakdown of hemoglobin (Hb)(Guo et al.,2020). Subsequently, as a result of excessive iron, a large number of reactive oxygen species were generated by damaged mitochondria(Lemasters et al.,2017), and the disturbance of glutamine metabolism lead to a functional decline of the antioxidant system, contributing to the production of hydroxyl radicals causing neuronal ferroptosis(Imai et al.,2017). Thus, neuronal ferroptosis can be reduced after ICH either by reducing excessive iron accumulation or by improving antioxidant system function(DeGregorio-Rocasolano et al., 2019;Magtanong et al.,2018).

The p62/Keap1/Nrf2 pathway plays an important role in protection of cells against ferroptosis-induced oxidative damage(Sun et al., 2016;Liu et al.,2016). Studies have shown that it is involved in the regulation of iron homeostasis and response to antioxidants(O'Connell et al.,2015). When exposed to the ferroptosis-inducing agent erastin, p62 expression increases nuclear factor erythroid 2-related factor 2 (Nrf2) nuclear accumulation and enhances the subsequent transcription of FTH1 and heme oxygenase-1 (HO1) by inhibiting Kelch-like ECH-associated protein 1 (Keap1) activation(Cloer et al., 2018). The former stores intracellular excess iron and reduces iron-dependent peroxidative damage, while the latter is an important antioxidant enzyme(Imam et al.,2017). Additionally, it is becoming apparent that Nrf2 plays a critical role in mitigating lipid peroxidation. Nrf2 controls the expression of ferritin and ferroportin(Sun et al.,2016). Furthermore, some important genes encoding proteins responsible for glutathione synthesis, including cystine/glutamate antiporter (system xc^-) and GPX4, are identified downstream targets of Nrf2(Fan et al.,2017;Kerins MJ et al.,2018). Interestingly, ferroptosis-inducing agents RSL-3 and erastin initiate the ferroptotic cascade by inhibiting them(Dodson et al.,2019;Kong et al.,2019). Collectively, this molecular pathway of scavenging oxidation products and free radicals caused by excess iron by activation of the p62/Keap1/Nrf2 pathway and subsequent nuclear accumulation of Nrf2, may serve as potential protection against ferroptosis after ICH(Chang et al., 2014).

Acupuncture, as a traditional treatment method, has been widely recognized by the medical community for its unique advantages in the treatment of cerebrovascular diseases(Schnyer et al.,2008). In the treatment of acute ICH, SA treatment proved to be safe and effective in improving clinical neurological function deficits and limb hemiplegia(Wang et al.,2016;Song et al.,2019;Liu et al.,2014;Han et al.,2019;Liu et al.,2019). A study on the time-effect relationship of acupuncture on histopathology, ultrastructure and neurological impairment of acute phase ICH found that the earlier the acupuncture intervention, the greater the improvement of neurological function, especially 3 or 9 hours after ICH in rats(Li et al.,2019). In addition, a meta-analysis and preclinical systematic review indicated that scalp penetration acupuncture at Baihui (DU20) may be an effective alternative therapy for acute ICH(Li et al.,2014). A series of studies revealed that SA could facilitate neurological functional recovery in a rat ICH model(Liu

et al.,2017), and that Baihui (DU20)-penetrating-Qubin (GB7) acupuncture can inhibit the activation of the Mincle/Syk signaling pathway, thereby reducing the release of proinflammatory cytokines(Liu et al.,2018), and that acupuncture can inhibit apoptosis, possibly by activating the Sonic hedgehog pathway(Zhang et al.,2018;Li et al.,2017). Furthermore, acupuncture may increase nerve repair capacity by inhibiting the Notch-Hes pathway and maintaining neural stem cell proliferation(Zou et al.,2015). Previous research has also found that acupuncture can promote resistance to oxidative stress injury by activating the Nrf2/ARE pathway(Zhao et al., 2019). However, whether SA treatment can activate the p62/Keap1/Nrf2 pathway involved in inhibiting ferroptosis after ICH remains unknown. Based on early evidence related to ICH treatment by acupuncture, this project intends to replicate the ICH rat model using Western blot, immunohistochemistry, electron microscopy, and other technologies to assess the effect of SA treatment on ferroptosis and elaborate its potential underlying mechanisms.

Materials And Methods

Animal studies. All experimental animals were purchased from the Laboratory Animal Center (under license No. SYXK (Hei) 2018-015). The use of live rats in research and teaching was approved by the local ethics committee of Heilongjiang University of Traditional Chinese Medicine of China (approval No. 2018-06-02-01).The experiments were carried out strictly in line with the requirements of the International Association for the Study of Pain (IASP)(Breivik et al.,2002). All rats were weighed and then anaesthetised by intraperitoneal injection of pentobarbital sodium (1%,60 mg/kg). Cervical dislocation was conducted at the end of life to ensure painless and ethical death. All experiments were conducted in accordance with the Guide of the US National Institutes of Health (revised in 1985 [publication No. 85–23]) for the Care and Use of Laboratory Animals. In total, 160 healthy male Sprague-Dawley (SD) rats (280 ± 10 g; 8-10-weeks-old) were housed in an environment at a temperature of 21 ± 2°C and relative humidity of 50 ± 5%, with a 12-hour light/dark cycle and free access to food and water. Following 1 week of adaptive feeding, rats were randomly divided into the control group (n = 32), the sham group (n = 32), the ICH model group (n = 32), the SA treatment group (n = 32) and the DFX group (n = 32). Each group was further divided into four subgroups (n = 8), which were sacrificed at 6 hours, 1 day, 3 days, and 7 days after ICH.With the exception of the control and sham group rats, the successful ICH model was confirmed by the Ludmila Belayev test and HE staining.

Model establishment. ICH was induced by stereotactic injection of autologous blood into the right basal ganglia(MacLellan et al.,2008). After preparing the skin and performing routine disinfection, rats were anaesthetized by intraperitoneal injection of pentobarbital (1%,60 mg/kg) and fixed on the stereotaxic apparatus (68001, RWD Life Science,Co.Ltd, Shenzhen, Guangdong Province, China). A midline incision was made by cutting the scalp longitudinally and a bone stripper was used to strip the periosteum, exposing the bregma and coronal suture. Using a dental drill, a 1.0 mm-diameter round hole was drilled at a point 3.5 mm lateral and 0.2 mm posterior to bregma until the dural surface(Khazipov et al.,2015). Autologous blood (50 μL) was collected with a microinjector from the tail vein and infused into the caudate putamen at a speed of 25 μL/min and at a depth of 6 mm. The microinjector was removed after 5 minutes. Finally, the scalp was sutured, the wound skull was blocked with zinc phosphate cement, and

the wounded tail was bandaged with gauze.Six hours after ICH, only rats with scores of 1 to 3 were selected as successful animal models and used in this study according to Berderson's scale(Bederson et al.,1986).

Group treatments . Rats in the SA treatment group (ICH + SA group) began receiving daily SA treatment for 30 minutes with the Baihui acupoint-penetrating-Qubin acupoint for 7 consecutive days after successful model establishment 6 hours. Rats in the model group (ICH group) received the same fixation as did the SA treatment group ,without acupuncture treatment. The DFX group rats (DFX being a ferroptosis inhibitor, ICH + DFX group) received daily intraperitoneal injections of DFX (100 mg/kg per day; 500 mg dissolved in 5 mL of 0.9% normal saline) (Novartis Pharmaceutical Co. LTD, Beijing, China) at the same frequency as acupuncture treatment in the SA treatment group. The DFX dosage was determined based on a previous report(Sun et al.,2016). Rats in the control and sham groups were included as controls as they did not receive any treatment. The same needle procedures as in the ICH group were performed in the sham group, but the same volume of saline was injected instead of blood. Every intervention was carried out continuously once a day until the animals were sacrificed.

Scale acupuncture treatment. Six hours after successful model establishment, rats in the SA treatment group began receiving daily SA treatment for 30 minutes. SA treatment was performed by experienced physicians with at least 3 months of training in rats. Based on previous works(Liu et al.,2017;Liu et al.,2018;Zhang et al.,2018), Baihui acupoint (DU20, in the middle between their two ears) and Qubin acupoint (GB7, leading edge of the tragus) on the side of the lesion were first accurately located. After routine skin disinfection, a sterile acupuncture needle (0.30 ×25 mm,Huatuo, Suzhou Medical Supplies Factory Co. LTD, Suzhou, China) was penetrated into the Baihui acupoint (DU20). The needle tip traveled subcutaneously along the direction from Baihui (DU20) to Qubin (GB7), piercing through the epicranial aponeurosis to a depth of 15 mm. The needle was subsequently rotated manually alternating between clockwise and counter-clockwise directions at a frequency of 180 ± 20 r/min for 5 minutes, intermittently for 5 minutes. The manual operation was performed a total of three times over the course of a 30-minute period.

Neurological function assessment. Neurological deficit scores were assessed at 6 hours, 1 day, 3 days, and 7 days after ICH using the Ludmila Belayev test(Belayev et al.,1996;De Ryck et al.,1989) by two experimenters who were blinded to the experimental design. Rats were evaluated for their postural reflex and placement test. The latter included visual, tactile and proprioception tests. Each item was graded from 0 to 2, establishing a maximum total deficit score of 12. The final score of each item was the average score given by the two experimenters. The higher the score, the more severe the neurological impairment. See **Supplementary file 1** for details.

Histopathological assay. Upon completion of the behavioral evaluation, rats were anesthetized with 1% pentobarbital and used for hematoxylin-eosin (H & E) staining. Following the perfusion with 4% paraformaldehyde, brain tissues around the lesions were sectioned into 5-μm slices to evaluate organizational structure. Images were captured under a microscope (BX53 Olympus Corporation, Tokyo,

Japan) at 200× magnification. The results of H & E staining were consistent with the pathological injury characteristics of cerebral hemorrhage, indicating the success of the model.

Transmission electron microscope (TEM). Rats in the sham group and rats at 3 days and 7 days after ICH were perfused with 2% paraformaldehyde and 2% glutaraldehyde in 0.1 M sodium cacodylate buffer, after which they were post-fixed in 2% osmium tetroxide with 1.6% potassium ferrocyanide in 0.1 M sodium cacodylate(Bogacz et al.,2018). Brain tissues in the perihemorrhagic area and the corresponding location in the sham group were then cut into 1 mm^3 clumps and stained en bloc with 2% uranyl acetate (UA), dehydrated in ethanol, and embedded in eponate. We stained semi-thin sections (0.5–2 um) with hematoxylin and eosin to identify the orientation and location (margins of hematoma) of the sections under a microscope. The sections (60–90 nm) were then placed on copper slot grids and stained with 2% UA and lead citrate. Micrographs were captured with a Hitachi H-7650 TEM at the Microscopy Center of Haerbin Medical University. In each rat, ten random micrographs were taken in the perihemorrhagic tissues and the corresponding location in the sham group for assessment of mitochondrial size using Image J software(National Institutes of Health,version1.8.0,). We measured the full mitochondrial area in the neuronal soma. Mitochondrial length was determined by measuring the maximum mitochondrial diameter. Data are presented as frequency distributions of the areas of mitochondria. Analysis was performed by an investigator blinded to treatment assignment.

Protein extraction and western blot analysis. After deep anesthesia and saline transcardial perfusion, fresh brain tissues were extracted and placed on ice, cut into 4-mm coronal slices, and stored in cryopreservation tubes at − 80°C for Western blot assay. Total protein was extracted by whole protein extraction kit (Wanleibio Biotechnology Co., LTD,WLA019,China) and the protein concentration was measured by BCA protein concentration kit (Wanleibio Biotechnology Co., LTD,WLA004,China). Thirty micrograms of protein (30 μg) were separated by SDS-PAGE and transferred to PVDF membranes (Millipore, Inc, IPVH00010, USA). Membranes were blocked in 5% skimmed milk for 1 hour after which they were immersed in Tris buffered saline with 0.1% Tween-20 and incubated with primary antibodies against NeuN (1:500, no.WL03099, 46 kDa, Wanleibio), Nrf2 (1:400,no.bs-1074R, 68 kDa,Bioss), FTH1 (1:1000, no.ab183781, 21 kDa, Abcam), GPX4 (1:500,no. ab125066, 22 kDa, Abcam), p62 (1:500,no. WL02385,50 kDa,Wanleibio), Keap1 (1:500,no.WL03285, 69 kDa, Wanleibio) and β-actin (1:1000, no.WL01845, Wanleibio) overnight at 4°C. Subsequently, samples were washed and incubated in goat-anti-rabbit IgG-HRP (1:5000,no.WLA023, Wanleibio) for 45 min at 37°C. Protein bands were evenly coated with luminescent liquid (Wanleibio Biotechnology Co., LTD) and exposed. Images were scanned, and optical density values of the target bands were analyzed usingGel-Pro-Analyzer software (MediaCybernetics, Inc.version 4.0,). All grayscale values were normalized to that of β-actin for statistical evaluation.

Immunohistochemical staining . Perihemorrhagic brain tissues were collected from rats in different groups after perfusion. After they were embedded in paraffin, tissues were cut into 5 μm sections and dewaxed with xylene. Next, the sections were immersed in the antigen repair solution and heated for 10 minutes under a low flame. When cooled to room temperature, the tissues were incubated in 3% hydrogen

peroxide and blocked with goat serum. At each step, sections were rinsed three times with phosphate-buffered saline (PBS) for 5 min. Subsequently, sections were incubated with primary antibodies, namely rabbit antiNrf2 (1:200,no. bs-1074R, Bioss), rabbit antiFTH1 (1:400,no. ab183781, abcam), and rabbit antiGPX4 (1:300,no.ab125066, abcam) overnight at 4°C. They were then incubated with the corresponding biotinylated goat anti-rabbit IgG (1:200,no. A0277, Beyotime) secondary antibody for 30 min at 37°C. Finally, tissues were labeled with horseradish, developed in DAB, immersed in distilled water, and counterstained with hematoxylin. Sections were then dehydrated and sealed. Images were obtained with a microscope (DP73, Olympus Corporation, Tokyo, Japan) at 400× magnification.

*MDA and Iron concentration measurement.*The relative concentrations of malondialdehyde (MDA) and Iron in perihemorrhagic brain tissues were detected with an MDA Assay Kit (Wanleibio Biotechnology Co., LTD, WLA048a, China) and an Iron Assay Kit (TC1015, Leagene Biotechnology Co. LTD, China) according to the manufacturer's instructions. MDA concentrations were measured at an optical density (OD) of 570 nm. Iron concentrations were measured at an optical density (OD) of 562 nm.

Statistical analysis. In this study, IBM SPSS statistics for windows (IBM Corp.,version 26.0 Armonk, NY, USA) was used for data analysis. Continuous data are expressed as means ± standard deviations (mean ± SD). Comparison among different groups at the same time point adopted one-way analysis of variance followed by post-hoc multiple comparisons of Tukey’s Honestly Significant Difference. A P value of < 0.05 was considered to be statistically significant.

Results

SA attenuates neurological function impairment in ICH rats.In order to investigate the effect of SA on neurological deficits, several behavioral experiments were performed post-ICH. We found that there were no significant differences in the test scores of subgroups between the control and sham groups(Fig. 1D;$P > 0.05$). However, the test data showed that the score was significantly higher in the ICH group than the control and sham groups (Fig. 1D;$P < 0.05$). Consistent with previous results(Guo et al.,2019),Neurological deficits were most apparent at 3 days after ICH. But DFX administration and SA significantly decreased neurological function deficits scores at 1 day and 3 days following ICH (Fig. 1D;$P < 0.05$). In addition, no significant differences were observed in scores between the SA and DFX administration groups (Fig. 1D;$P > 0.05$). These results indicated that SA attenuates neurological function impairment in ICH rats.

SA attenuates pathological injury in ICH rats. Hematoxylin-eosin staining was performed to examine histological changes in rats (Fig. 1A). Brain tissues in the sham and control groups showed normal microscopic features, without inflammatory infiltration, edema, dead neurons from the semi-dark area. However, the ICH rats showed a large number of inflammatory cells, red cells and broken cells, which was accompanied by edema, disordered cellular architecture, severe vacuolation of the intercellular space, neuronal karyopyknosis, and anachromasis in neurons at 3days. However, SA treatment improved pathological injury post-ICH; in other words, the blood was absorbed obviously and a small amount of infiltrated red cells and inflammatory cells and was associated with neurological functional recovery.

SA treatment attenuates ferroptosis related characteristic mitochondrial morphology in ICH rats.To confirm that SA treatment attenuates ferroptosis, we observed the mitochondria structure of the neuronal soma in the perihematoma region by transmission electron microscope(Li et al.,2018;Lewerenz et al.,2018). As shown in (Fig. 2C), neuronal soma show a large number of shrunken mitochondria (red arrowheads) at 3 days post-ICH even with increased mitochondrial membrane density and the rupture of outer mitochondrial membrane. We further measured the area of all mitochondria in neuronal somas in all images. Analyses revealed that there was a higher frequency of smaller mitochondrial areas in the somas at both 3 days and 7 days after ICH.(Fig. 2A and B). However ,compared with the ICH group, neuronal soma show scattered shrunken mitochondria (red arrowheads) with thickened and ruptured outer mitochondrial membrane at 3 days after SA treatment and DFX administration. In order to further observe the cumulative effect of SA treatment, we observed the changes of neuron mitochondria at 7 days. As shown in (Fig. 2D), atrophic and ruptured mitochondria were still observed in the neurons of brain tissue in the perihematoma of ICH rats. However, compared with the ICH group, the mitochondria of neurons are basically normal, with a small amount of swollen mitochondria, indicating mild damage of neurons at 7 days after SA treatment and DFX administration. These results indicated that SA treatment attenuates ferroptosis-related mitochondrial morphology.

SA treatment increases NeuN expression in ICH rats .To confirm that neurons were vulnerable to ICH injury, we observed the expression of NeuN by Western blot (Fig. 3A). ICH caused substantial neuronal death at 3 days and 7 days compared with the sham group, but DFX and SA treatments significantly rescued neurons under these conditions. Expression levels of NeuN were significantly higher in the SA treatment and DFX groups than the ICH group (Fig. 3C;$P < 0.05$). There were no significant differences in NeuN expression levels between SA and DFX groups (Fig. 3C;$P > 0.05$). Therefore, SA treatment had effects on neuronal protection.

SA treatment alleviates ICH-induced MDA accumulation by increasing GPX4 expression .As shown in(Fig. 1C;$P < 0.05$), results of the absorbance of samples revealed that the levels of MDA in perihematomal regions increased significantly in the ICH group compared with the sham group. However, SA and DFX treatment decreased the levels of MDA in perihematoma compared with the ICH group. No significant differences in MDA levels were observed between the SA and DFX administration groups (Fig. 1C;$P > 0.05$), indicating that SA attenuates MDA accumulation in ICH rats.

Oxidative stress is one of the key elements in secondary ICH injury(Zhang et al., 2018). GPX4 is one of the important antioxidant enzymes in oxidative stress balance(Li et al.,2018), and GPX4 levels after ICH are decreased, exacerbating neuronal ferroptosis lipid peroxidation injury(Wu et al.,2013;Wenzel et al.,2017). To further confirm the relationship between GPX4 and MDA accumulation in ICH brain, we assessed the presence of GPX4-positive cells. GPX4 immunopositivity indicated that GPX4 decreased from 6 hours to 3 days after ICH injury and significantly increased in the SA group (Fig. 4A and D;$P < 0.05$). Western blot analyses further demonstrated that GPX4 expression was upregulated after SA treatment compared with the ICH group at different time points (Fig. 3B and F;$P < 0.05$). Taken together, these results indicate that SA effectively attenuates ICH-induced brain oxidative injury by increasing GPX4 expression.

SA treatment alleviates ICH-induced iron accumulation by increasing FTH1 expression. As shown in (Fig. 1B;$P < 0.05$), the total iron levels in perihematomal regions continued to rise after ICH, peaking at 3 days, and maintaining high levels at 7 days compared with the sham group. However, SA and DFX treatment decreased iron concentrations in perihematomal regions compared with the ICH group(Fig. 1B;$P < 0.05$),. No significant differences in iron content were observed between the SA treatment and DFX administration groups (Fig. 1B;$P > 0.05$), indicating that SA attenuates iron accumulation in ICH rats.

A series of studies reported that iron-binding protein FTH1 participate in regulating iron homeostasis after ICH(Yang et al.,2016;Bogdan et al.,2016). To investigate the mechanisms involved in alleviating iron overload, we next examined FTH1 expression. Compared with the sham group, ICH resulted in increased iron levels at 6 hours, 1 day, 3 days, and 7 days after ICH (Fig. 1B;$P < 0.05$). At the same time, ICH resulted in an increase in FTH1-positive cells at these corresponding time points. Interestingly, compared with the ICH group, the number of FTH1-positive cells increased significantly (Fig. 4A and C;$P < 0.05$)and iron levels decreased significantly in the SA treatment group. The relationship between FTH1 and iron accumulation was further confirmed by Western blot. The results confirmed that FTH1 protein levels were higher at various time points in brain tissues following SA when compared with the ICH group (Fig. 3B and E;$P < 0.05$). These results revealed that SA treatment alleviates ICH-induced iron accumulation by increasing FTH1 expression. To identify whether the higher FTH1 expression levels contributed to alleviating neuronal lipid peroxidation injury caused by iron over-accumulation, we measured MDA at 3 days post-ICH, when oxidative injury reached its maximum. Results revealed that iron accumulation reached its peak at 3 days after ICH, when oxidative injury in brain tissues was most severe. Taken together, these results indicate that SA can effectively alleviate neuronal lipid peroxidation injury caused by iron over-accumulation by increasing FTH1 expression.

SA treatment may increases FTH1 and GPX4 levels by enhancing nuclear accumulation of Nrf2.Nrf2 is an important regulator under conditions of oxidative challenge(Kang et al.,2017), and GPX4 and FTH1 are the key downstream effectors of Nrf2. To test whether SA treatment increases the levels of FTH1 and GPX4 by enhancing nuclear accumulation of Nrf2, we assessed Nrf2 immunopositivity in the brain by immunohistochemistry. The number of Nrf2-positive cells increased significantly in the SA treatment group compared with the ICH group, and nuclear Nrf2 accumulation increased significantly at 1 day and 3 days post-ICH (Fig. 4Aand B;$P < 0.05$;). At the same time, GPX4 and FTH1 immunopositivity results were consistent with altered Nrf2 levels(Fig. 4Aand C;Fig. 4Aand D;)

To further confirm these results, we assessed protein expression levels of Nrf2 and downstream transcripts GPX4 and FTH1 by Western blot, which revealed similar results (Fig. 3Band D-F;). Taken together, these results suggested that SA may increased FTH1 and GPX4 levels by enhancing Nrf2 nuclear accumulation.

SA treatment promotes Nrf2 transcription by enhancing the interaction between p62 and Keap1. Recently, studies have demonstrated that the substrate adaptor p62 protein (also called sequestosome 1) directly

regulated Nrf2 expression by binding Keap1 under conditions of stress, including liver damage(Shen et al.,2018) and head and neck cancer(Roh et al.,2017). To better understand the mechanisms underlying ICH-induced Nrf2 upregulation, we detected p62 and Keap1 protein expression levels by Western blot (Fig. 5A-C). The expression levels of p62 increased in brain tissues of ICH rats, whereas Keap1 protein levels decreased. Moreover, compared with the ICH group, SA treatment was able to significantly increase p62 protein expression and decrease Keap1 protein expression at 1 day and 3 days after ICH (Fig. 5B and C;$P < 0.05$;). These results suggest a binding reaction between p62 and Keap1, especially after SA treatment. Next, we investigated whether p62 binds Keap1 to displace Nrf2, thus inhibiting Nrf2 degradation and enhancing nuclear accumulation. The Western blot results suggested that Nrf2 levels increased dramatically in early stages as p62 levels increased and Keap1 levels decreased (Fig. 3B and D;$P < 0.05$;). These results showed that the increase in Nrf2 expression was related to the interaction between p62 and Keap1. Collectively, these results suggested that the interaction between p62 and Keap1 was responsible for Nrf2 nuclear accumulation in ferroptosis and that SA treatment may promote Nrf2 transcription by enhancing the interaction between p62 and Keap1.

Discussion

Intracerebral hemorrhage (ICH) is a devastating disease and is always followed by several types of cell death. However, the therapeutic strategies targeting currently known cell death pathways fail to effectively improve neurological deficits after ICH. As a new form of cell death, ferroptosis is closely related to neurological deficits after ICH. Ferroptosis is a recently reported form of programmed cell death that plays an important role in tumors, ICH, ischemia reperfusion injury, kidney degeneration, and other diseases(Stockwell et al.,2017;Sarhan et al.,2018). Because iron and lipid metabolisms are associated with ICH pathophysiology, we speculated that ferroptosis plays a key role in ICH secondary injury. In the present study, we observed over-accumulation of iron and lipid peroxidation products as well as specific ferroptosis-related shrunken mitochondria in the somas of perihemorrhagic brain tissue. Moreover, we found that SA treatment reduced ICH-induced neurological impairment by inhibiting ferroptosis, similar to the protective effects of DFX(Hu et al.,2019). Notably, we provided evidence that SA treatment protects the hemorrhagic brain by enhancing the p62/Keap1/Nrf2 antioxidative signaling pathway, a key regulator of ferroptosis by transcriptional activation of genes involved in ROS and iron metabolism. SA treatment may be developed into a potential clinical therapy for ICH patients.

A previous study has shown that iron overload plays a pathogenic role in oxidative brain injury(Magtanong et al.,2018). After ICH, iron concentrations can reach high levels, accelerating the generation of free radicals via Fenton reactions(Li et al.,2017). In our research, we found that the concentrations of iron and MDA were upregulated, reaching their highest levels 3 days after ICH. At the same time, ferroptosis mitochondria underwent signs of morphological changes, including decreased ridges, ruptured outer membranes, and reduced size. These data strongly re-confirm the fact that ferroptosis does occur in cerebral hemorrhage tissues. Moreover, SA downregulated the concentrations of iron and MDA, reducing iron overload and lipid peroxidation. Considering that the changes in iron and MDA are consistent, we speculated that SA may alleviate oxidative damage by reducing the

accumulation of excess iron. Given the characteristics of ferroptosis(Dixon et al.,2012) and the role of Nrf2 regulation, we focused on analyzing protein expression levels of Nrf2, which is involved in both iron metabolism and ROS metabolism, and sought to elucidate the mechanisms underlying SA treatment.

Nrf2 is an important regulator under conditions of oxidative challenge and may be critical in protecting against ferroptosis(Abdalkader et al.,2018). A previous study has found that Nrf2 nuclear accumulation can reduce early brain injury in ICH brain(Zhao et al.,2007;Zeng et al.,2017) and further confirmed that Nrf2 KO mice have a larger ICH-induced lesion volume and more iron-loaded cells than do WT mice 72 hours post-ICH(Chang et al.,2014). Under unstressed conditions, Nrf2 persists in an inactivated state through Keap1-mediated ubiquitination and degradation in the proteasome(Fan et al.,2017;Toyokuni et al.,2014). In our study, we found that Nrf2 expression remains low in normal brain tissue. After ICH, with the emergence of oxidative stress, Nrf2 levels gradually increased. Nrf2 levels reached their peak when iron overload and oxidative damage were most severe at 3 days. In addition, immunohistochemical results showed that not only the expression but also the nuclear accumulation of Nrf2 reached peak values at 3 days. We know that Nrf2 has many target genes encoding a variety of detoxification and antioxidant proteins such as GPX4(Fischer et al.,2019). As previously described, GPX4 is a mammalian selenoprotein glutathione peroxidase with a crucial role in repairing oxidative damage to lipids(Yang et al.,2014). Other studies have shown that a lack of GPX4 triggered motor neuron degeneration in the spinal cord, characterized by ferroptosis, and that GPX4 was essential for motor neuron survival(Chen et al.,2015). In addition, we also found that the lower the level of GPX4, the more serious the oxidative damage related to ferroptosis(Zhang et al.,2018). When GPX4 reached its lowest level at 3 days after ICH, significant changes in ferroptosis mitochondria were observed. Other studies further proved that genetic-overexpression of GPX4 effectively increased level of GPX4 and clearly relieved neuronal dysfunction and oxidative stress after ICH. In contrast, inhibiting GPX4 with a specific pharmacological inhibitor or genetic knockdown exacerbated SBI after ICH(Zhang et al.,2018). Besides, FTH1 is another key gene regulated by Nrf2. Ferritin is the key iron binding protein in the brain consisting of two subunits (FTH1/FTL) of which FTH1 has the activity of ferrous oxidase and is mainly involved in the rapid uptake and re-utilization of iron and FTL mainly helps to maintain the stability of ferritin, which is related to the long-term storage of iron in cells(Liu et al.,2013). Animal experiments have shown that compared with sham group rats, FTH1 levels were significantly higher after ICH(Yang et al.,2016). Our data indicated that FTH1 expression in normal brain tissues remained low, gradually increasing along with increased iron accumulation after ICH. After SA treatment, with the increase of FTH1, the level of iron decreased, indicating that SA may promote the expression of FTH1 and further promote the uptake and re-utilization of the iron. Interestingly, the trends in the levels of FTH1 and GPX4 were consistent with those of Nrf2 levels. Here, we proved that the expression of FTH1 and GPX4 in ICH brain is closely related to the transcription of Nrf2. Nrf2 activation may be critical in countering the effects of the reduced GPX4 activity(Kerins et al.,2018). Moreover, similar to Nrf2 knockdown, FTH1 knockdown can also enhance ferroptosis sensitivity(Sun et al.,2016;Fan et al.,2017). The above mentioned studies provide empirical support that Nrf2 may be a dependent transcription to regulate the level of GPX4 and FTH1. In our experiment, scalp acupuncture is

likely to promote the expression of FTH1 and GPX4 by Nrf2 dependent pathway, further promoting the uptake and utilization of excess iron, reducing iron overload and further lipid peroxidation injury.

In order to study the mechanisms of Nrf2 nuclear accumulation, we carried out additional research. Data from other groups has shown that p62 protein serves as a multi-functional scaffold protein that plays a role in a number of signal transduction pathways(Sánchez-Martín et al.,2018). Nrf2 is kept in check by keap1-dependent degradative ubiquitination(Hassannia et al.,2018).Under conditions of stress, p62 interacts with the Nrf2-binding site of Keap1 and competitively inhibits the binding of Keap1 and Nrf2, which is responsible for Nrf2 nuclear accumulation(Xie et al.,2016). Furthermore, a previous study has shown that the p62/Keap1/Nrf2 antioxidative signaling pathway is involved in protection against ferroptosis(Sun et al.,2016;Fischer et al.,2019). Therefore, we speculated that Nrf2 disengages from binding Keap1 and translocates to the nucleus, subsequently binding antioxidant response elements of target genes against various injuries. In line with this, our experimental western blot results revealed that the antioxidant effect of Nrf2 was accompanied by an increase in p62 expression and decrease in Keap1 expression. Moreover, SA treatment can enhance the binding of p62 and Keap1, increase the accumulation of Nrf2 nucleus, and promote antioxidant effects.

In conclusion, our findings provided evidence that SA treatment protects the brain against early ferroptosis lipid peroxidation injury, probably by activating a switch in the p62/Keap1/Nrf2 pathway antioxidant system, promoting subsequent Nrf2 nuclear accumulation .On the one hand, SA treatment can enhance the expression of FTH1, promote the utilization of excess iron, and reduce the production of oxidation products. On the other hand, it can enhance the expression of GPX4 and promote the elimination of oxidation products, thereby consisting of a promising therapy for ICH.

Although we have provided evidence for the mechanisms underlying SA treatment protects against neuronal ferroptosis lipid peroxidation in ICH models, additional research efforts are warranted. Currently, there is lack of specific markers to detect ferroptosis. However, in our study, we did not detect any ferroptosis-related genes. We provided a strong support through the specific mitochondrial morphology changes of ferroptosis, as well as iron overload, and accumulation of lipid peroxidation products to verify the occurrence of ferroptosis. Further detection of changes in gene levels may be more convincing. In addition, in our study, we found that the phenomenon of improvement of ferroptosis lipid peroxidation of nerve cells after SA treatment is related to the transcription of Nrf2 by Western Blot and immunohistochemistry. There is no use of specific gene-deficient rats (e.g., Nrf2 knockout [KO]) or related inhibitors, which cannot fully prove that acupuncture causes Nrf2 dependent expression of FTH1 and GPX4 in brain tissues after ICH. Studies examining the effect of Nrf2 activation *in vitro* models of ferroptosis would provide some insight. In addressing this question, We believe that our findings will provide a vital foundation for cell death-based ICH treatment in the future.

Declarations

Acknowledgments

Not applicable.

Funding

This study was supported by the National Natural Science Foundation of China (Grant No. 81473764,81273824); the Key Project of Natural Science Foundation of Heilongjiang Province of China, No. ZD201204; the Doctoral Fund Program of Ministry of Education of China, No.20102327110003.The funding body played no role in the study design; collection, analysis, and interpretation of data; writing of the paper; and decision to submit the paper for publication.

Availability of data and materials

The datasets used and/or analyzed during the current study are available from the corresponding author on reasonable request.

Authors' contributions

MYL and WZ designed the experiments. MYL, QA, and XW carried out the experiments. XHD and XPY collected the data. WT, PL, and XYY analyzed the data. MYL, XHD, and PL wrote the manuscript. XYY, XPY, and WZ revised the manuscript. All authors approved the final version of the paper.

Ethics approval and consent to participate

The use of live rats in research and teaching was approved by the local ethics committee of Heilongjiang University of Traditional Chinese Medicine of China (approval No. 2018-06-02-01).The experiments were carried out strictly in line with the requirements of the International Association for the Study of Pain (IASP). All experiments were conducted in accordance with the Guide of the US National Institutes of Health (revised in 1985 [publication No. 85–23]) for the Care and Use of Laboratory Animals

Patient consent for publication

Not applicable.

Competing interests

The authors have no conflicts of interest to declare.

References

1. Abdalkader M, Lampinen R, Kanninen KM, Malm TM, Liddell JR (2018) Targeting Nrf2 to suppress ferroptosis and mitochondrial dysfunction in neurodegeneration. Front Neurosci 12:466.
2. Buccarelli M, Marconi M, Pacioni S, Pascalis ID, D'Alessandris QG, Martini M, Ascione B, Malorni W, Larocca LM, Pallini R, Ricci-Vitiani L, Matarrese P(2018)

3. Inhibition of autophagy increases susceptibility of glioblastoma stem cells to temozolomide by igniting ferroptosis. Cell Death Dis 9:841.
4. Breivik H(2002)International Association for the study of pain: Update on WHOIASP activities. J Pain Symptom Manage 24: 97–101.
5. Belayev L, Alonso OF, Busto R, Zhao W, Ginsberg MD. (1996) Middle cerebral artery occlusion in the rat by intraluminal suture. Neurological and pathological evaluation of an improved model. Stroke 27:1616-22
6. Bederson JB, Pitts LH, Tsuji M, Nishimura MC, Davis RL, Bartkowski H(1986) Rat middle cerebral artery occlusion: evaluation of the model and development of a neurologic examination. Stroke 17:472-6.
7. Bogacz M, Krauth-Siegel RL(2018) Tryparedoxin peroxidase-deficiency commits trypanosomes to ferroptosis-type cell death. Elife 7:e37503.
8. Bogdan AR, Miyazawa M, Hashimoto K, Tsuji Y (2016) Regulators of iron homeostasis: new players in metabolism, cell death, and disease. Trends Biochem Sci 41:274 – 86.
9. Cloer EW, Siesser PF, Cousins EM, Goldfarb D, Mowrey DD, Harrison JS, Weir SJ,Dokholyan NV, Major MB(2018) p62-dependent phase separation of patient-derived KEAP1 mutations and NRF2. Mol Cell Biol 38: e00644-17.
10. Chang CF, Cho S, Wang J (2014) (-)-Epicatechin protects hemorrhagic brain via synergistic Nrf2 pathways.Ann Clin Transl Neurol 1:258 – 71.
11. Chen L, Hambright WS, Na R, Ran Q(2015) Ablation of the ferroptosis inhibitor glutathione peroxidase 4 in neurons results in rapid motor neuron degeneration and paralysis. J Biol Chem 290:28097-106
12. Devos D, Moreau C, Kyheng M, Garçon G, Rolland AS, Blasco H, Gelé P, Timothée Lenglet T, Veyrat-Durebex C, Corcia P, Dutheil M, Bede P, Jeromin A, Oeckl P, Otto M, Meininger V, Danel-Brunaud V, Devedjian JC, Duce JA, Pradat PF(2019) A ferroptosis-based panel of prognostic biomarkers for amyotrophic lateral sclerosis. Sci Rep 9:2918.
13. DeGregorio-Rocasolano N, Martí-Sistac O, Gasull T(2019) Deciphering the iron side of stroke: neurodegeneration at the crossroads between iron dyshomeostasis, excitotoxicity, and ferroptosis. Front Neurosci 13:85.
14. Dodson M, Castro-Portuguez R, Zhang DD (2019) NRF2 plays a critical role in mitigating lipid peroxidation and ferroptosis. Redox Biol 11:101107.
15. De Ryck M, Van Reempts J, Borgers M, Wauquier A, Janssen PA(1989) Photochemical stroke model: flunarizine prevents sensorimotor deficits after neocortical infarcts in rats. Stroke 20:1383-90.
16. Dixon SJ, Lemberg KM, Lamprecht MR, Skouta R, Zaitsev EM, Gleason CE, Patel DN, Bauer AJ, Cantley AM, Yang WS, Morrison B 3rd, Stockwell BR (2012)
17. Ferroptosis: an iron-dependent form of nonapoptotic cell death. Cell 149:1060-72.

18. Fan Z, Wirth AK, Chen D, Wruck CJ, Rauh M, Buchfelder M, Savaskan N(2017) Nrf2-Keap1 pathway promotes cell proliferation and diminishes ferroptosis. Oncogenesis 6:e371.
19. Fischer W, Currais A, Liang Z, Pinto A, Maher P(2019) Old age-associated phenotypic screening for Alzheimer's disease drug candidates identifies sterubin as a potent neuroprotective compound from Yerba santa. Redox Biol 21:101089.
20. Guo X, Qi X, Li H, Duan Z, Wei Y, Zhang F, Tian M, Ma L,You C(2019)Deferoxamine Alleviates Iron Overload and Brain Injury in a Rat Model of Brainstem Hemorrhage.World Neurosurg 128:e895-e904.
21. Guo X, Ma L, Li H, Qi X, Wei Y, Duan Z, Xu J, Wang C, You C ,Tian M(2020)Brainstem iron overload and injury in a rat model of brainstem hemorrhage.J Stroke Cerebrovasc Dis 29:104956.
22. Haller JT, Wiss AL, May CC, Jones GM, Smetana KS(2019)Acute management of hypertension following intracerebral hemorrhage. Crit Care Nurs Q 42:129 – 47.
23. Han X, Bai LJ, Sun CZ, Niu X, Ning YZ, Chen Z, Li YY,Li KS, Lyu DY,Fu CH,Cui FY,Chen ZG,Tan ZJ,Tang LX,Zou YH (2019) Acupuncture enhances communication between cortices with damaged white matters in poststroke motor impairment. Evid Based Complement Alternat Med2019:4245753.
24. Hu S, Hua Y, Keep RF, Feng H,Xi G(2019)Deferoxamine therapy reduces brain hemin accumulation after intracerebral hemorrhage in piglets.Exp Neurol 318:244–250.
25. Hassannia B, Wiernicki B, Ingold I, Qu F, Herck SV, Tyurina YY, Bayır H, Abhari BA, Friedmann Angeli JP, Choi SM, Meul E, Heyninck K, Declerck K, Chirumamilla CS, Lahtela-Kakkonen M, Camp GV, Krysko DV, Ekert PG, Fulda S, De Geest BG, Conrad M, Kagan VE, Berghe WV,Vandenabeele P, Berghe TV (2018)Tyurina Nano-targeted induction of dual ferroptotic mechanisms eradicates high-risk neuroblastoma. J Clin Invest 128:3341-55.
26. Imam MU, Zhang S, Ma J, Wang H, Wang F(2017) Antioxidants mediate both iron homeostasis and oxidative stress. Nutrients 9:671.
27. Imai H, Matsuoka M, Kumagai T, Sakamoto T, Koumura T (2017) Lipid peroxidation-dependent cell death regulated by GPX4 and ferroptosis. Curr Top Microbiol Immunol 403:143 – 70.
28. Kerins MJ, Ooi A(2018) The roles of NRF2 in modulating cellular iron homeostasis. Antioxid Redox Signal 29:1756-73.
29. Kong Z, Liu R, Cheng Y (2019) Artesunate alleviates liver fibrosis by regulating ferroptosis signaling pathway. Biomed Pharmacother109:2043-53.
30. Khazipov R, Zaynutdinova D, Ogievetsky E, Valeeva G, Mitrukhina O, Manent JB, Represa A(2015) Atlas of the postnatal rat brain in stereotaxic coordinates. Front Neuroanat 9:161.
31. Kang R, Tang D(2017) Autophagy and ferroptosis - what's the connection? Curr Pathobiol Rep 5:153-9.
32. Kerins MJ, Milligan J,Wohlschlegel JA ,Ooi A(2018)Fumarate hydratase inactivation in hereditary leiomyomatosis and renal cell cancer is synthetic lethal with ferroptosis Induction. Cancer Sci 109: 2757-66.

33. Li Q, Han X, Lan X, Gao Y, Wan J, Durham F, Cheng T, Yang J, Wang Z, Jiang C, Ying M, Koehler RC, Stockwell BR, Wang J (2017)Inhibition of neuronal ferroptosis protects hemorrhagic brain. JCI Insight 2:e90777.
34. Lemasters JJ (2017) Evolution of voltage-dependent anion channel function: from molecular sieve to governator to actuator of ferroptosis. Front Oncol 7:303.
35. Liu WJ, Ye L, Huang WF, Guo LJ, Xu ZG, Wu HL,Yang C,Liu HF(2016) P62 links the autophagy pathway and the ubiqutin-proteasome system upon ubiquitinated protein degradation. Cell Mol Biol Lett 21:29.
36. Liu X, Bao C, Dong G (2014)Using acupoint-to-acupoint penetrative needling to treat post-stroke spastic paralysis: a clinical progress review. J Tradit Chin Med 34:609 – 15.
37. Liu SN, Zhang CS, Cai YY, Guo XF, Zhang AL, Xue CC, Lu CJ(2019) Acupuncture for post-stroke shoulder-hand syndrome: a systematic review and meta-analysis. Front Neurol 10:433.
38. Li ZW, Zheng XN, Li P(2019)Time-effect relationship of acupuncture on histopathology, ultrastructure, and neuroethology in the acute phase of cerebral hemorrhage. Neural Regen Res 14:107 – 13.
39. Li HQ, Li JH, Liu AJ, Ye MY, Zheng GQ(2014) GV20-based acupuncture for animal models of acute intracerebral haemorrhage: a preclinical systematic review and meta-analysis. Acupunct Med 32:495–502.
40. Liu H, Sun XW, Zou W, Leng MT, Zhang B, Kang XY, He T,Wang H (2017) Scalp acupuncture attenuates neurological deficits in a rat model of hemorrhagic stroke. Complement Ther Med 32:85–90.
41. Liu XY, Dai XH, Zou W, Yu XP, Teng W, Wang Y, Yu WW, Ma HH, Chen QX, Liu P, Guan RQ, Dong SS(2018) Acupuncture through Baihui (DU20)to Qubin (GB7) mitigates neurological impairment after intracerebral hemorrhage. Neural Regen Res 13:1425–1432.
42. Li Z, Zheng X, Li P, Itoua ES, Moukassa D, Ndinga Andely F(2017) Effects of acupuncture on mRNA levels of apoptotic factors in perihematomal brain tissue during the acute phase of cerebral hemorrhage. Med Sci Monit 23:1522-32.
43. Li Q, Weiland A, Chen XM, Lan X, Han XN, Durham F,Liu X,Wan JR, Ziai WC, Hanley DF, Wang J(2018) Ultrastructural characteristics of neuronal death and white matter injury in mouse brain tissues after intracerebral hemorrhage: coexistence of ferroptosis, autophagy, and necrosis. Front Neurol 9:581.
44. Lewerenz J, Ates G, Methner A, Conrad M, Maher P(2018) Oxytosis/ferroptosis-(re-) emerging roles for oxidative stress-dependent non-apoptotic cell death in diseases of the central nervous system. Front Neurosci 12:214.
45. Li C, Deng X, Xie X, Liu Y, Friedmann Angeli JP, Lai L(2018) Activation of glutathione peroxidase 4 as a novel anti-inflammatory strategy. Front Pharmacol 9:1120.
46. Li Q, Wan J, Lan X, Han X, Wang Z, Wang J(2017) Neuroprotection of brain-permeable iron chelator VK-28 against intracerebral hemorrhage in mice. J Cereb Blood Flow Metab 37:3110-23.

47. Liu HD, Li W, Chen ZR, Zhou ML, Zhuang Z, Zhang DD,Zhu L, Hang CH(2013) Increased expression of ferritin in cerebral cortex after human traumatic brain injury. Neurol Sci 34:1173-80.
48. Müller T, Dewitz C, Schmitz J, Schröder AS, Bräsen JH, Stockwell BR, Murphy JM, Kunzendorf U, Krautwald S(2017) Necroptosis and ferroptosis are alternative cell death pathways that operate in acute kidney failure. Cell Mol Life Sci 74:3631-45.
49. Masaldan S, Bush AI, Devos D, Rolland AS, Moreau C(2019) Striking while the iron is hot: iron metabolism and ferroptosis in neurodegeneration. Free Radic Biol Med 133:221 – 33.
50. Magtanong L, Dixon SJ (2018) Ferroptosis and brain injury. Dev Neurosci 40:382 – 95.
51. MacLellan CL, Silasi G, Poon CC, Edmundson CL, Buist R, Peeling J,Colbourne F(2008) Intracerebral hemorrhage models in rat: comparing collagenase to blood infusion. J Cereb Blood Flow Metab 28:516 – 25.
52. O'Connell MA, Hayes JD(2015) The Keap1/Nrf2 pathway in health and disease: from the bench to the clinic. Biochem Soc Trans 43:687-9.
53. Bai Q,Liu J,Wang G(2020)Ferroptosis, a Regulated Neuronal Cell Death Type After Intracerebral Hemorrhage. Front Cell Neurosci 14:591874
54. Roh JL, Kim EH, Jang H, Shin D(2017) Nrf2 inhibition reverses the resistance of cisplatin-resistant head and neck cancer cells to artesunate-induced ferroptosis. Redox Biol 11:254 – 62.
55. Rocha E, Rouanet C, Reges D, Gagliardi V, Singhal AB,Silva GS(2020)Intracerebral hemorrhage: update and future directions. Arq Neuropsiquiatr,78:651–659.
56. Speer RE, Karuppagounder SS, Basso M, Sleiman SF, Kumar A, Brand D, Smirnova N, Gazaryan I, Khim SJ, Ratan RR (2013) Hypoxia-inducible factor prolyl hydroxylases as targets for neuroprotection by "antioxidant" metal chelators: from ferroptosis to stroke. Free Radic Biol Med 62:26–36.
57. Sun X, Ou Z, Chen R, Niu X, Chen D, Kang R, Tang DL (2016) Activation of the p62-Keap1-NRF2 pathway protects against ferroptosis in hepatocellularcarcinoma cells. Hepatology 63:173 – 84.
58. Sun X, Niu X, Chen R, He W, Chen D, Kang R, Tang DL (2016) Metallothionein-1G facilitates sorafenib resistance through inhibition of ferroptosis. Hepatology 64:488–500.
59. Schnyer R, Lao L, Hammerschlag R, Wayne P, Langevin HM, Napadow V,Harris R, Park J, Milley R, Cohen M, MacPherson H (2008) Society for Acupuncture Research: 2007 conference report: "The status and future of acupuncture research: 10 years post-NIH Consensus Conference". J Altern Complement Med 14:859 – 60.
60. Song GF, Wu CJ, Dong SX, Yu CH, Li X(2019) Rehabilitation training combined acupuncture for limb hemiplegia caused by cerebral hemorrhage: a protocol for a systematic review of randomized controlled trial. Medicine (Baltimore) 98:e14726.
61. Sun YM, Wang YT, Jiang L, Xue MZ(2016)The effects of deferoxamine on inhibition for microglia activation and protection of secondary nerve injury after intracerebral hemorrhage in rats.Pak J Pharm Sci. 29:1087-93.

62. Shen Z, Wang Y, Su Z, Kou R, Xie K ,Song F(2018)Activation of p62-keap1-Nrf2 antioxidant pathway in the early stage of acetaminophen-induced acute liver injury in mice.Chem Biol Interact 82:22–28.
63. Stockwell BR, Friedmann Angeli JP, Bayir H, Bush AI, Conrad M, Dixon SJ, Fulda S, Gascón S, Hatzios SK, Kagan VE, Noel K, Jiang XJ, Linkermann A, Murphy ME, Overholtzer M, Oyagi A, Pagnussat GC, Park J, Ran Q, Rosenfeld CS, Salnikow K, Tang D, Torti FM, Torti SV, Toyokuni S, Woerpel KA, Zhang DD (2017) Ferroptosis:a regulated cell death nexus linking metabolism, redox biology, and disease. Cell 171:273 – 85.
64. Sarhan M, von Mässenhausen A, Hugo C, Oberbauer R, Linkermann A (2018) Immunological consequences of kidney cell death. Cell Death Dis 9:114.
65. Sánchez-Martín P ,Komatsu M(2018) p62/SQSTM1 - steering the cell through health and disease.J Cell Sci.131:jcs222836.
66. Toyokuni S(2014) Iron and thiols as two major players in carcinogenesis: friends or foes? Front Pharmacol 5:200.
67. Tan X, Yang Y,Xu JG, Zhang P, Deng RM, Mao YG, He J, Chen YB, Zhang Y, Ding JH, Li HY, Shen HT, Li X, Dong WL, Chen G(2020)
68. Luteolin Exerts Neuroprotection via Modulation of the p62/Keap1/Nrf2 Pathway in Intracerebral Hemorrhage.Front Pharmacol 10:1551.
69. Weimar C, Kleine-Borgmann J(2017) Epidemiology, prognosis and prevention of non-traumatic intracerebral hemorrhage. Curr Pharm Des 23:2193-6.
70. Wang HQ, Bao CL, Jiao ZH, Dong GR(2016) Efficacy and safety of penetration acupuncture on head for acute intracerebral hemorrhage: a randomized controlled study. Medicine (Baltimore) 95:e5562.
71. Wu G, Sun S, Sheng F, Wang L, Wang F(2013) Perihematomal glutamate level is associated with the blood-brain barrier disruption in a rabbit model of intracerebral hemorrhage. Springerplus 2:358.
72. Wenzel SE, Tyurina YY, Zhao J, St Croix CM, Dar HH, Mao G,Tyurin VA, Anthonymuthu TS, Kapralov AA, Amoscato AA, Mikulska-Ruminska K, Shrivastava IH, Kenny EM, Yang Q, Rosenbaum JC, Sparvero LJ, Emlet DR, Wen X, Minami Y, Qu F, Watkins SC, Holman TR, VanDemark AP, Kellum JA, Bahar I, Bayır H, Kagan VE(2017) PEBP1 wardens ferroptosis by enabling lipoxygenase generation of lipid death signals. Cell 171:628 – 41.e26.
73. Xie Y, Hou W, Song X, Yu Y, Huang J, Sun X, Kang R, Tang D(2016) Ferroptosis: process and function. Cell Death Differ 23:369 – 79.
74. Yang WS, SriRamaratnam R, Welsch ME, Shimada K, Skouta R, Viswanathan VS, Cheah JH, Clemons PA, Shamji AF, Clish CB, Brown LM, Girotti AW, Cornish VW, Schreiber SL, Stockwell BR(2014) Regulation of ferroptotic cancer cell death by GPX4. Cell 156:317 – 31.
75. Yao X, Zhang Y, Hao J, Duan HQ, Zhao CX, Sun C, Li B, Fan BY, Wang X, Li WX, Fu XH, Hu Y, Liu C, Kong XH, Feng SQ (2019)Deferoxamine promotes recovery of traumatic spinal cord injury by inhibiting ferroptosis. Neural Regen Res 14:532 – 41.
76. Yang G, Hu R, Zhang C, Qian C, Luo QQ, Yung WH, Ke Y, Feng H,Qian ZM(2016)A combination of serum iron, ferritin and transferrin predicts outcome in patients with intracerebral hemorrhage.Sci

Rep 6:21970.

77. Zille M, Kumar A, Kundu N, Bourassa MW, Wong VSC, Willis D, Karuppagounder SS, Ratan RR (2019) Ferroptosis in neurons and cancer cells is similar but differentially regulated by histone deacetylase inhibitors. eNeuro 6:ENEURO.0263-18.2019.
78. Zhang Z, Wu Y, Yuan S, Zhang P, Zhang J, Li H, Li X, Shen H ,Wang Z, Chen G(2018)Glutathione peroxidase 4 participates in secondary brain injury through mediating ferroptosis in a rat model of intracerebral hemorrhage. Brain Res 1701:112 – 25.
79. Zhang B, Dai XH, Yu XP, Zou W, Teng W, Sun XW,Yu WW, Liu H, Wang H, Sun MJ, Li M(2018) Baihui (DU20)-penetrating-Qubin (GB7) acupuncture inhibits apoptosis in the perihemorrhagic penumbra. Neural Regen Res13:1602-8.
80. Zou W, Chen QX, Sun XW, Chi QB, Kuang HY, Yu XP, Dai XH(2015) Acupuncture inhibits Notch1 and Hes1 protein expression in the basal ganglia of rats with cerebral hemorrhage. Neural Regen Res 10:457 – 62.
81. Zhao X, Sun G, Zhang J, Strong R, Dash PK, Kan YW, Grotta JC, Aronowski J(2007) Transcription factor Nrf2 protects the brain from damage produced by intracerebral hemorrhage. Stroke 38:3280-6.
82. Zhao X, Liu L,Wang Y,Wang G, Zhao Y, Zhang Y(2019)Electroacupuncture enhances antioxidative signal pathway and attenuates neuropathic pain induced by chemotherapeutic paclitaxel.Physiol Res 68:501–510.
83. Zeng J, Chen Y, Ding R, Feng L, Fu Z, Yang S, Deng X, Xie Z,Zheng S(2017)Isoliquiritigenin alleviates early brain injury after experimental intracerebral hemorrhage via suppressing ROS- and/or NF-κB-mediated NLRP3 inflammasome activation by promoting Nrf2 antioxidant pathway.J Neuroinflammation 14:119.

Figures

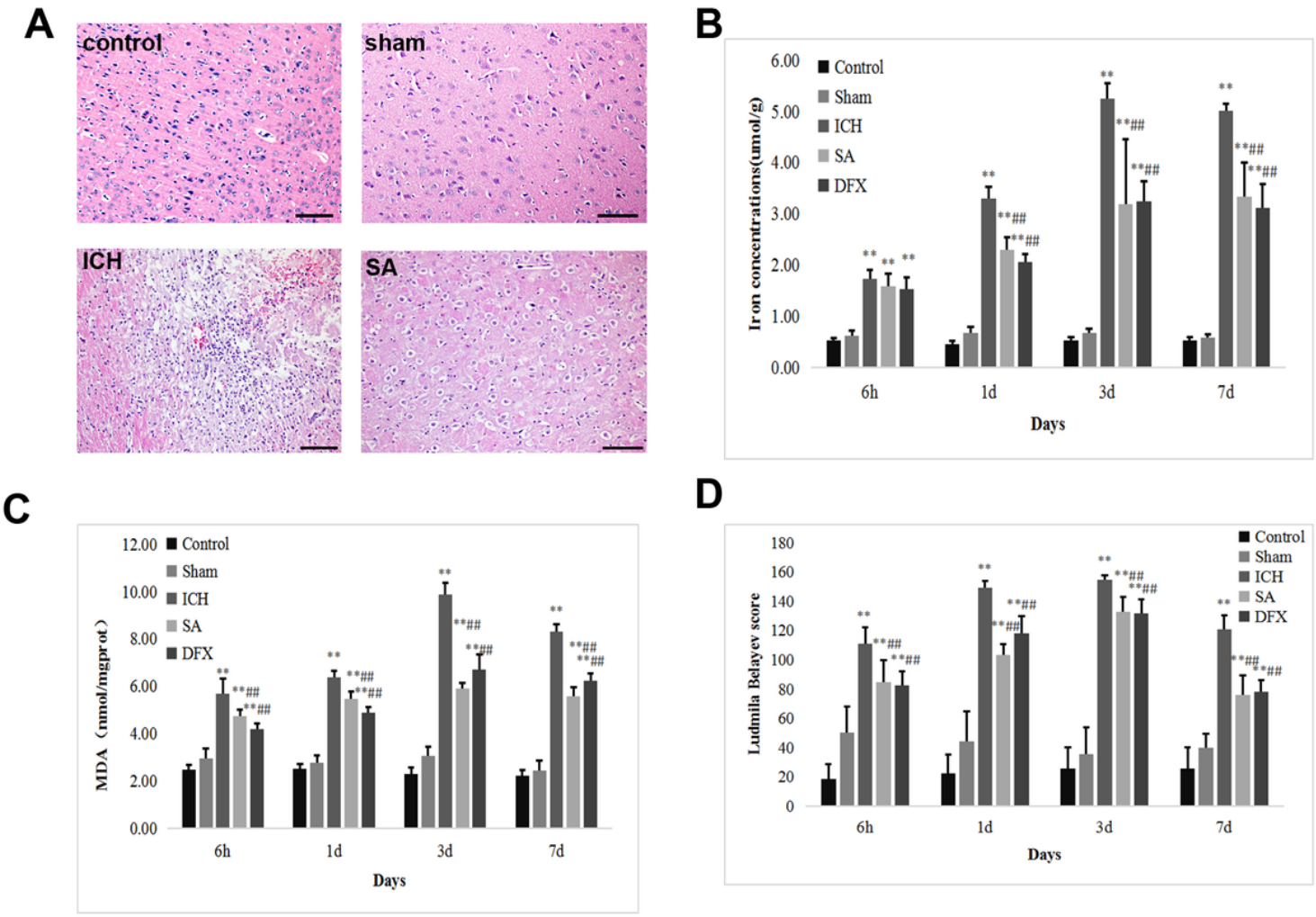

Figure 1

SA treatment attenuated pathological changes and neurological function impairment in ICH rats. (A) Representative images are shown under four different conditions at 3 days after ICH. Brain tissues in perihematomal regions of ICH rats were stained with hematoxylin-eosin (H & E) and examined under an Olympus fluorescence microscope (200× magnification).The red arrow indicates blood exudation, the blue arrow indicates nuclear pyknosis and disappearance, the yellow arrow indicates cell swelling and nuclear pyknosis, and the green arrow indicates inflammatory cell infiltration. SA treatment reduced the levels of (B) Fe , (C) MDA and attenuated (D) neurological function scores in ICH rats. Data are expressed as mean±SD (n = 8; **P < 0.05 vs. sham group; ##P < 0.05 vs. ICH group.Scale bar: 100 μm; ICH: intracerebral hemorrhage; SA: scalp acupuncture; DFX: desferrioxamine; h: hour(s); d: day(s)

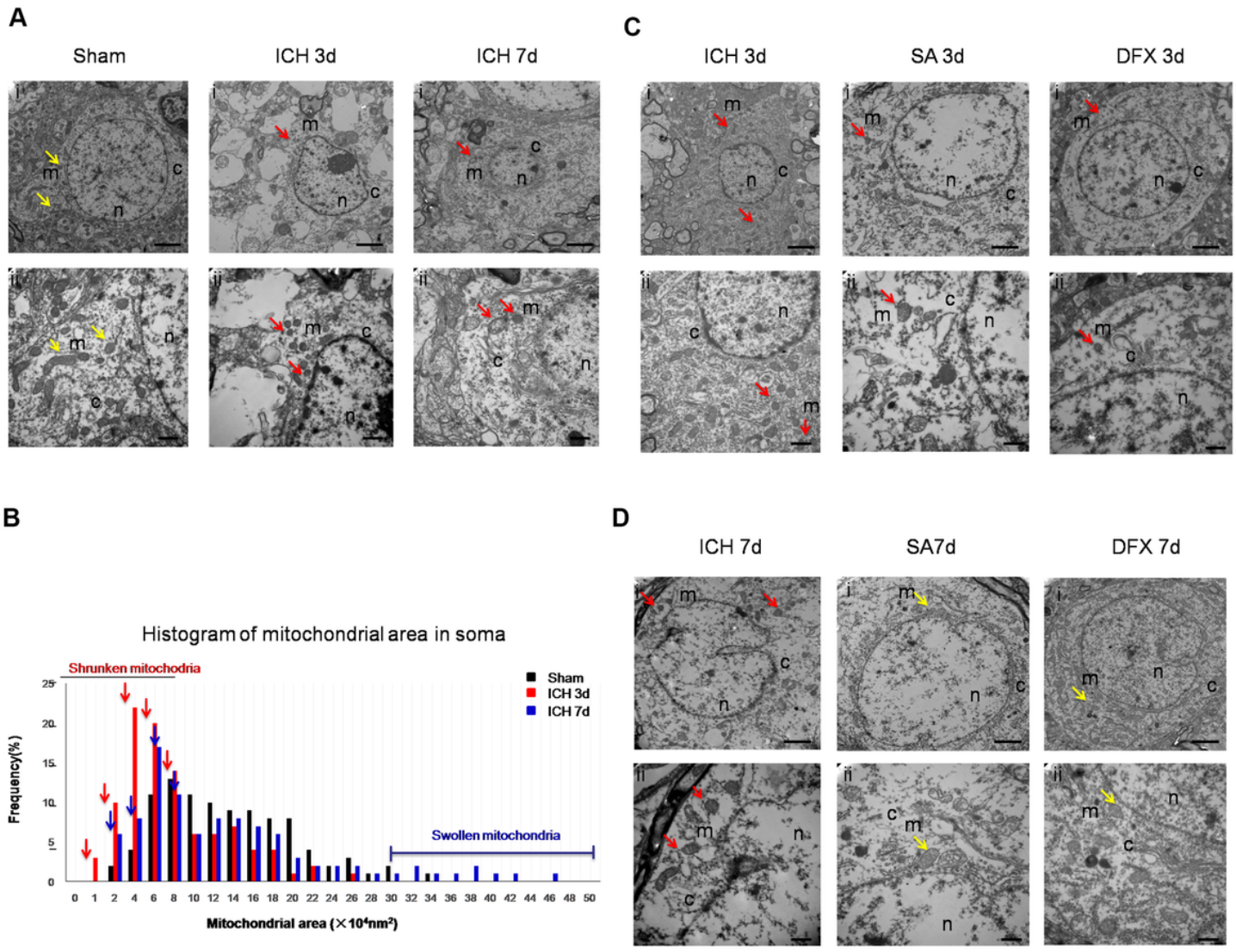

Figure 2

SA treatment attenuated ferroptosis related characteristic mitochondrial morphology in ICH rats. (A) The ultrastructure of neuronal somas showed signs of ferroptosis with evidence of shrunken mitochondria (red arrows) at 3 days and 7 days after ICH. (B) Quantification of the frequency of various mitochondrial areas in neuronal somas in the sham group at 3 days and 7 days after ICH. Arrows indicated the increased frequency of shrunken mitochondria on days 3 and 7. Number of mitochondria in the soma: sham, n = 206; ICH day 3, n = 153; ICH day 7, n = 171. SA treatment attenuates mitochondria structure of the neuronal soma in the perihematoma region at (C) 3 daysand (D) 7 days post ICH ,SA treatment, and

DFX administration. Scale bars: (Ai) 2 μm; (Aii) 500 nm.Red arrows indicate shrunken mitochondria;Yellow arrows indicate normal mitochondria.n , nucleus; c, cytoplasm; m, mitochondria; n = 3 animals per group

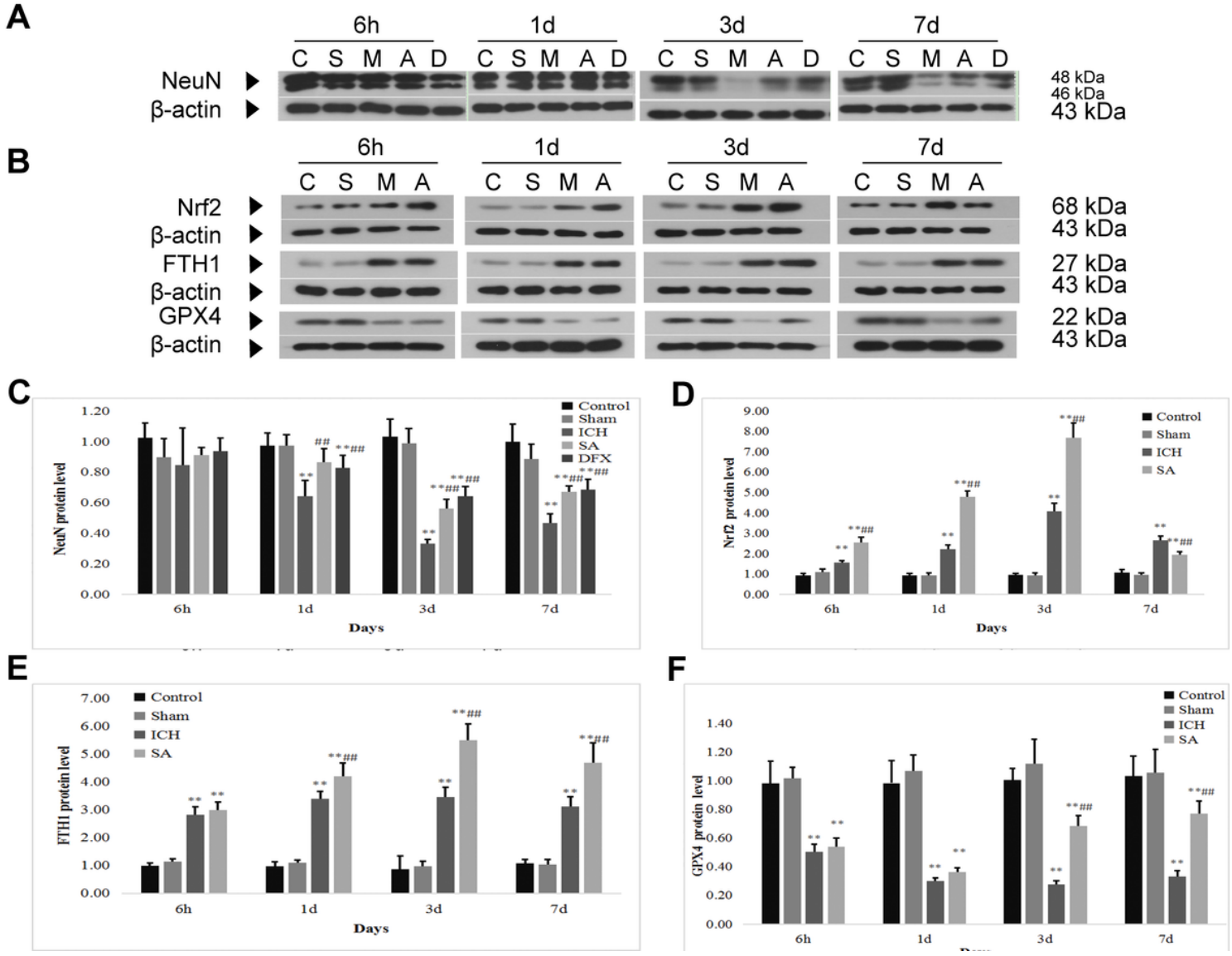

Figure 3

SA treatment decreased oxidative damage and attenuates neuronal cell death in ICH rats. Protein levels of (A)NeuN and (B)Nrf2,FTH1,GPX4were determined by Western blotting . Protein levels were normalized to the loading control β-actin. C: control group; S: sham group; M: ICH group; A: scalp acupuncture group; D: DFX group; Quantitative analysis of protein expression levels of (C) NeuN,(D)Nrf2,(E)FTH1 and (F)GPX4. Data are presented as mean±SD (n = 8; **P < 0.05 vs. sham group; ##P < 0.05 vs. ICH group.ICH: intracerebral hemorrhage. SA: scalp acupuncture. DFX: desferrioxamine; Nrf2: nuclear factor erythroid 2-related factor 2; GPX4: glutathione peroxidase 4; FTH1: ferritin heavy chain 1 h: hour(s); d: day(s)

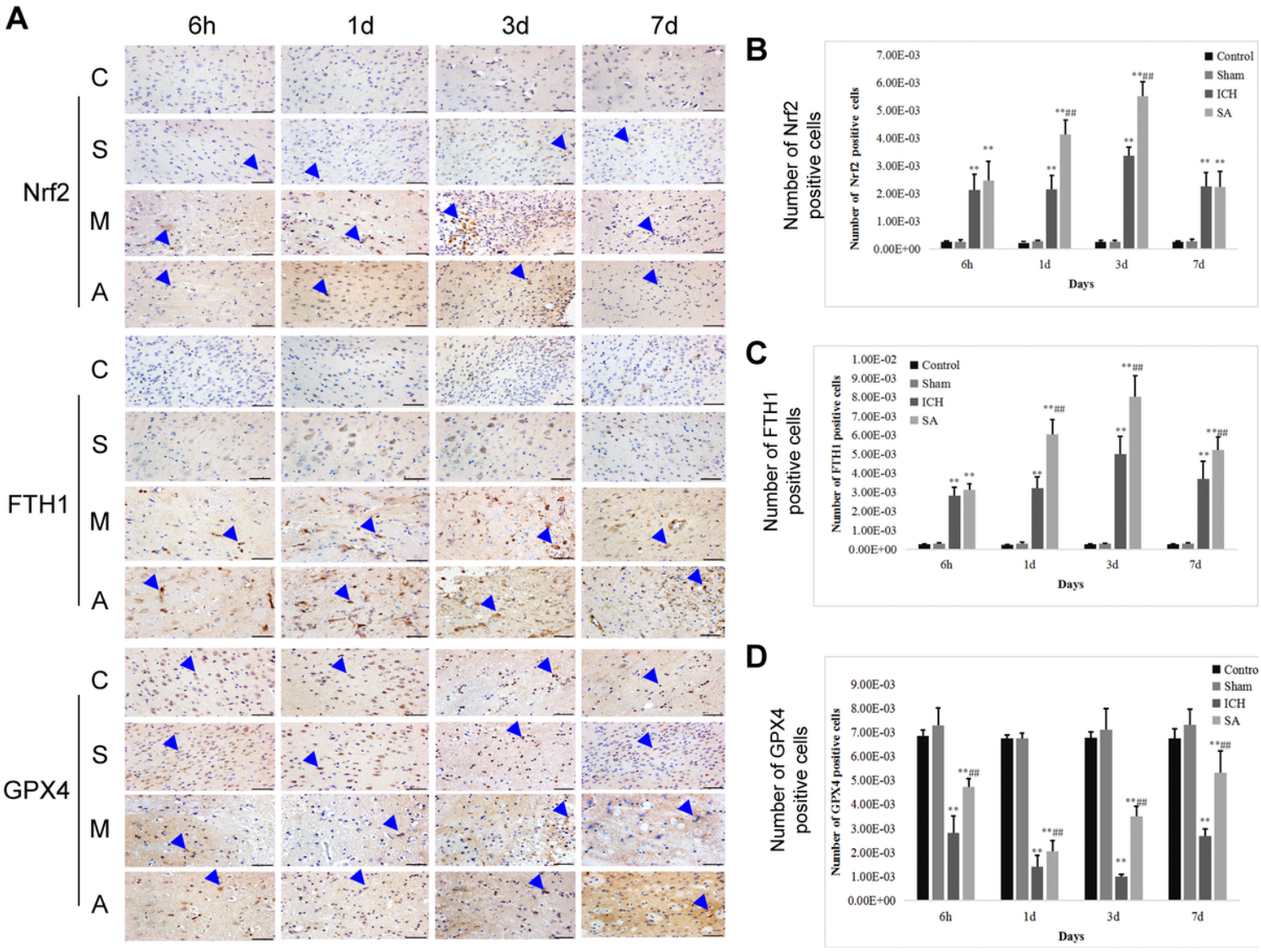

Figure 4

SA treatment increased nuclear accumulation of Nrf2 and attenuates oxidative damage in ICH rats. (A)The number of positive cells of Nrf2,GPX4 and FTH1 in rat brains at different time points after ICH were determined by immunohistochemistry. Immunohistochemical staining of brain tissue (original magnification, 200×). Positive cells are indicated by arrows. Scale bars: 100 μm. C:control group. S: sham group. M: ICH group. A: scalp acupuncture group. Number of (B)Nrf2-(C)FTH1-(D)GPX4-positive cells in 200-fold fields. Data are presented as mean±SD (n=8; **P < 0.05 vs. sham group; ##P < 0.05 vs. ICH group.) ICH: intracerebral hemorrhage; SA: scalp acupuncture;Nrf2: nuclear factor erythroid 2-related factor 2; GPX4: glutathione peroxidase 4; FTH1: ferritin heavy chain 1 h: hour(s); d: day(s)

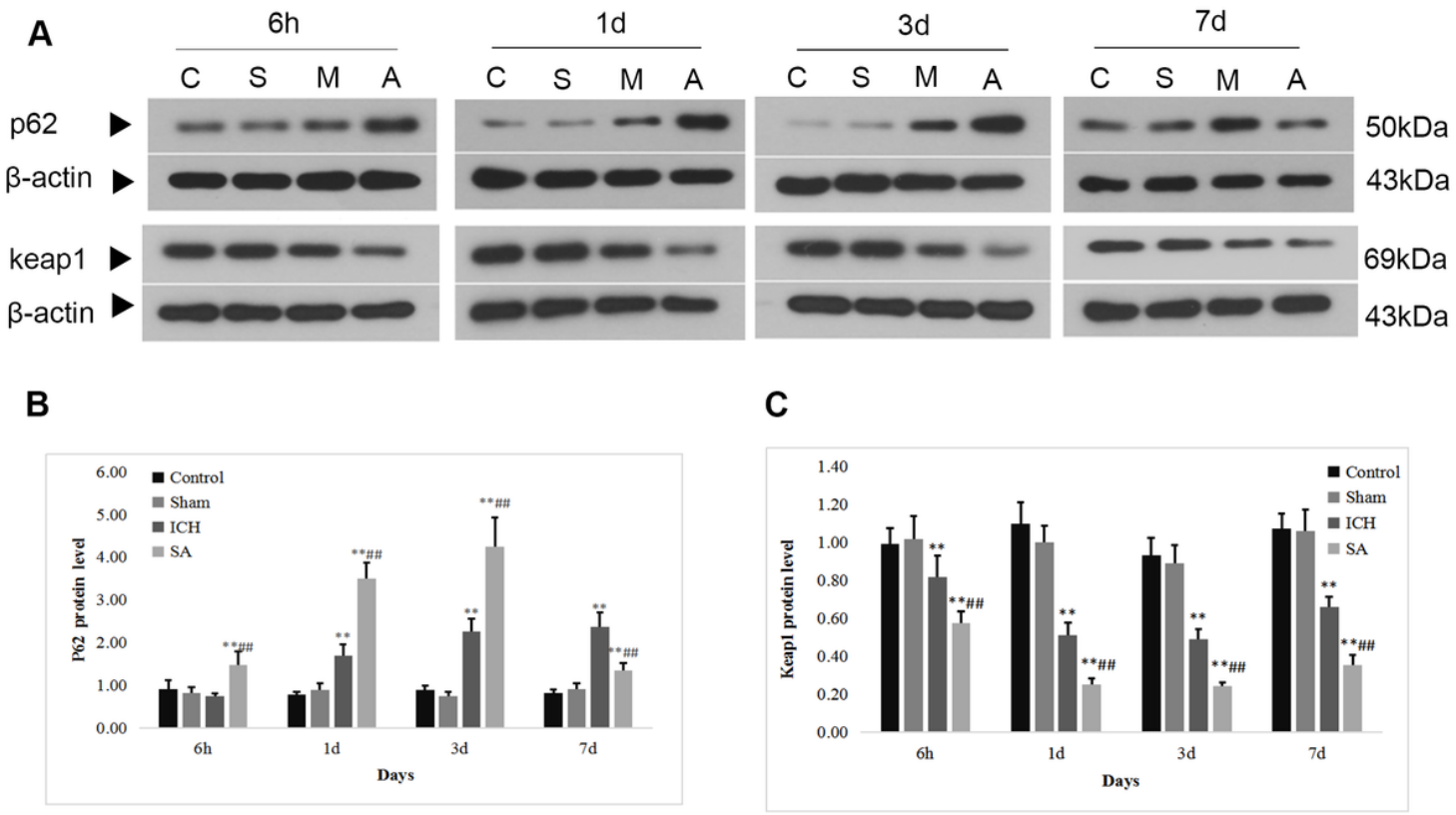

Figure 5

SA treatment promotes the p62 /Keap1/nrf2 pathway in ICH rats (A) Protein levels of p62 and keap1were determined by Western blotting . Protein levels were normalized to the loading control β-actin. C: control group; S: sham group; M: ICH group; A: scalp acupuncture group; Quantitative analysis of protein expression levels of (B) P62 and (C)keap1. Data are presented as mean±SD (n = 8; **P < 0.05 vs. sham group; ##P < 0.05 vs. ICH group.ICH: intracerebral hemorrhage. SA: scalp acupuncture. p62:Sequestosome 1 (p62/SQSTM1);keap1: Kelch-like ECH-associated protein-1; h: hour(s); d: day(s)

Supplementary Files

This is a list of supplementary files associated with this preprint. Click to download.

- Supplementaryfile1.docx